Vibrational Spectroscopy and Electron−Phonon Interactions in Microwave-Hydrothermal Synthesized Ba(Mn$_{1/3}$Nb$_{2/3}$)O$_3$ Complex Perovskites

Anderson Dias,*,† Franklin M. Matinaga,‡ and Roberto L. Moreira‡

Departamento de Química, Universidade Federal de Ouro Preto, Campus Morro do Cruzeiro, ICEB II, Sala 67, Ouro Preto-MG, 35400-000, Brazil, and Departamento de Física, ICEx, Universidade Federal de Minas Gerais, C.P. 702, Belo Horizonte-MG, 30123-970, Brazil

Ba(Mn$_{1/3}$Nb$_{2/3}$)O$_3$ ceramics were synthesized by the microwave-hydrothermal process. Crystalline, single-phase, needle-like materials were obtained with high anisotropy and aspect ratio. Large crystals could be prepared from a direct combination of nanosized crystals under microwaves through an oriented attachment mechanism. Infrared and Raman spectroscopies showed perfect agreement with group-theoretical approaches for a trigonal, $P\bar{3}m1$ structure. Franck−Condon modes were identified in Raman scattering experiments conducted in different wavelengths, laser powers, and temperatures. The results showed that the Mn ions exhibit a particular role in the lattice dynamics in complex perovskites.

1. Introduction

It is well-known that compounds with perovskite structure are the most interesting materials aiming to functional, applicable oxides.[1] An incredibly wide array of structures and phases with totally different functions can be prepared by using a combination of chemical elements in the basic formula ABO$_3$. Generally, transition metal ions are located in the center of symmetric oxygen octahedra (B-sites) that, in turn, are surrounded by larger ions forming an A-site ion cube. The multiple cation substitution in the perovskite lattice in either A or B positions, or in both, creates the so-called complex perovskites, which present pairs of unlike valence cations in proportions depending on their oxidation states and ionic radii.[1] In practice, most real perovskites display symmetry breaking due to displacements of the crystallographic sites from the ideal cubic positions. In this sense, a vast number of "tailor-made" compounds are being studied by the scientific community in the framework of their crystal chemistry toward emerging applications: ferroelectrics,[2] superconductors,[3] relaxors,[4] photonics,[5] catalysts,[6] and microwave dielectrics.[7]

Complex perovskites of the type A(B′$_{1/3}$B″$_{2/3}$)O$_3$ are frequently investigated, like Ba(Mg$_{1/3}$Ta$_{2/3}$)O$_3$ and Ba(Zn$_{1/3}$Ta$_{2/3}$)O$_3$, as they possess excellent microwave properties.[7] For this particular application, only the ceramic Ba(Zn$_{1/3}$Ta$_{2/3}$)O$_3$ is commercially available for frequencies in the gigahertz range.[7] In view of the high costs associated with tantalum oxide, the research changed the focus to cheaper niobium materials. Our group has studied many complex perovskites containing niobium in B-sites to contribute to the understanding of the relationship between chemical composition, crystal structure, and physical properties.[8−11] In particular, we showed that processing conditions influence directly extrinsic factors like microstructure, defects, and porosity, which in turn limit the applicability of these materials.[8−11] Our efforts are always toward environmentally friendly conditions for the processing of complex perovskite ceramics. In these respects, hydrothermal processes allow one to produce nanostructured, crystalline powders in a single step.[12] Moreover, the use of microwave heating of the hydrothermal solutions enhances the kinetics of crystallization, allowing the production of electroceramics in relatively shorter times.[8−12] Previous papers[8,11] showed that the hydrothermal method produces materials with high long-range order parameters, which are critical for minimum dielectric losses in microwave applications.

In this work, we introduce the microwave-hydrothermal synthesis of complex Ba(Mn$_{1/3}$Nb$_{2/3}$)O$_3$ ceramics. For this material, a few publications present crystal structure and vibrational spectroscopic data of conventionally prepared samples.[13,14] Infrared spectroscopy and Raman scattering are powerful tools to investigate crystal structures and vibrational properties of ceramic materials, allowing the determination and assignment of the phonon modes through factor-group analysis. For complex double perovskites containing Mn and W, the appearance of Franck−Condon modes in polarized resonance Raman scattering was reported recently.[15,16] In view of that, it is our goal to investigate the vibrational properties of complex Ba(Mn$_{1/3}$Nb$_{2/3}$)O$_3$ ceramics (BMnN) by both infrared and Raman spectroscopies, paying attention to the possible electron−phonon interactions. The role of the Mn ions in the lattice dynamics was studied by exciting the materials with different wavelengths, laser powers, and temperatures.

2. Experimental Section

BaCl$_2$·2H$_2$O and MnCl$_2$·6H$_2$O (>99%, Fluka Chemie AG, Switzerland), as well as NH$_4$H$_2$[NbO(C$_2$O$_4$)$_3$]·3H$_2$O (>99%, CBMM, Brazil), were used as reagents to synthesize BMnN. The salts were dissolved separately in deionized water (18.2 MΩ·cm) and mixed under stirring. The niobium ammonium oxalate was previously treated with a NaOH solution maintained at pH > 13 and washed to remove ammonia. After mixing, the precipitation occurred, and the pH was controlled and adjusted with NaOH to 13.5. BMnN ceramics were synthesized by the microwave-hydrothermal process, using a Milestone MLS-1200 MEGA microwave digestion system (2.45 GHz), according to procedures described in previous papers.[8,12] The materials were produced under microwaves at 200 °C, for 2 h, and the resulting

* Corresponding author. Tel.: +55-31-3559-1716. E-mail: anderson_dias@iceb.ufop.br.
† Universidade Federal de Ouro Preto.
‡ Universidade Federal de Minas Gerais.

powders were repeatedly washed with deionized water and dried at 80 °C. Calcined powders were produced by heating in a conventional muffle at 1000 °C, for 4 h, under air atmosphere. The powders were uniaxially pressed at 110 MPa and sintered in air at 1400 °C, for 4 h.

The crystal structure and phase purity of the as-synthesized samples were studied by X-ray diffraction technique (XRD) using a Shimadzu D-6000 diffractometer with graphite monochromator and a nickel filter in the 2θ range 10−100° (step 0.02°2θ), operating with Fe Kα radiation ($\lambda = 0.19360$ nm). The results were automatically converted to Cu Kα radiation for data treatment and manipulation. Transmission and scanning electron microscopes (Philips FEI-CM200 and JEOL 5410) were employed to study the morphological features of the powders after processing. Infrared reflectance spectra were recorded in a Fourier-transform spectrometer (Bomem DA 8-02) equipped with a fixed-angle specular reflectance accessory (external incidence angle of 11.5°). In the mid-infrared region (500 to 4000 cm^{-1}), we used a SiC glow-bar lamp as an infrared source, a Ge-coated KBr beamsplitter, and an LN$_2$-cooled HgCdTe detector. In the far-infrared range (50−600 cm^{-1}), we employed a mercury-arc lamp, a 6 μm coated Mylar hypersplitter, and an LHe-cooled Si-bolometer. One of the ceramic faces received a thin gold coating and was used as a "rough" mirror for the reference spectra. This procedure allowed us to improve the reflectivity spectra since the mirror surface mimics the sample one, which compensates the effects of diffuse reflection at the sample surface. The measurements were performed at a pressure of 10^{-4} bar and a resolution of 2 cm^{-1}.

Raman spectra were collected in backscattering configuration by using three different configurations. The first one was a triple-monochromator Dilor XY spectrometer with an Olympus confocal microscope (80× objective), exciting lines of 488 and 514.5 nm of an Ar$^+$ laser (effective powers from 10 to 50 mW at the sample's surface), and a liquid-N$_2$-cooled charge coupled device (CCD) detector. The frequency resolution was better than 2 cm^{-1}, and the accumulation times were typically 10 collections of 30 s. The second piece of equipment employed was a triple-monochromator Jobin-Yvon T64000 spectrometer, equipped with a liquid-N$_2$-cooled CCD detector and an Olympus BXL microscope (100× and 20× objectives, for room and varying temperatures, respectively), with a 532 nm line (second harmonic line of a YVO$_4$:Nd laser) as an excitation source (10−50 mW), and accumulation times of typically 10 collections of 30 s, with spectral resolution better than 2 cm^{-1}. Low- and high-temperature measurements were conducted in this equipment, either in a controlled (Lakeshore) coldfinger cryostat (Janis) or in a homemade microfurnace. Finally, a Horiba/Jobin-Yvon LABRAM-HR spectrometer was used with the 632.8 nm line of a helium−neon ion laser (effective power of 6 mW at the sample's surface) as an excitation source, diffraction gratings of 600 and 1800 grooves/mm, Peltier-cooled CCD detector, confocal Olympus microscope (100× objective), and experimental resolution of typically 1 cm^{-1} for 10 accumulations of 30 s. All resulting spectra were corrected by the Bose−Einstein thermal factor.[17]

3. Results

Microwave-hydrothermal processing produced crystalline, single-phase powders. Figure 1 presents the XRD for the ceramic sintered at 1400 °C, for 4 h, indexed with the ICDD card #46-0998. Very narrow, intense diffraction peaks can be visualized, and no impurities or secondary phases were detected. The sintered BMnN ceramic could be assumed as presenting a
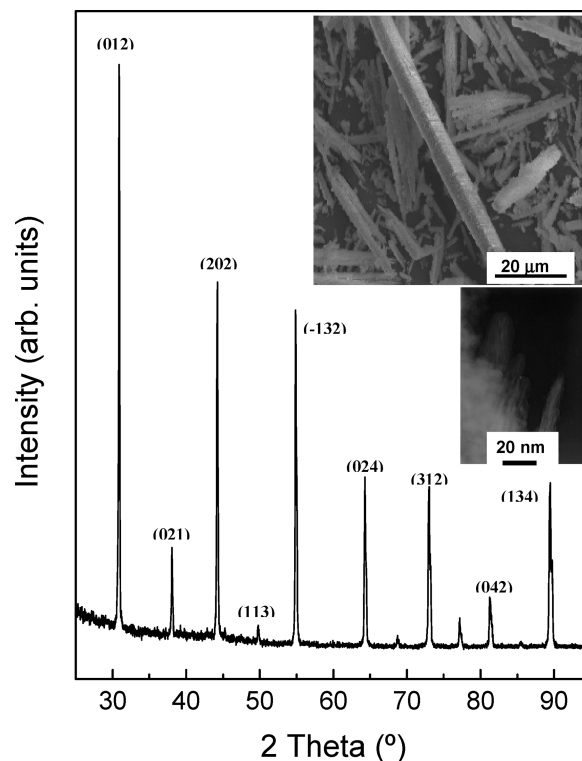

Figure 1. XRD pattern for the Ba(Mn$_{1/3}$Nb$_{2/3}$)O$_3$ ceramics sintered at 1400 °C, for 4 h. Insets: SEM and TEM images for the as-synthesized BMnN powders (source: Fe Kα, automatically converted to Cu Kα).

fully 1:2 ordered structure (trigonal, $P\bar{3}$m1, $a = b = 5.812$ Å and $c = 7.137$ Å), as also verified by Liu et al.[13] SEM and TEM images are also showed as insets in Figure 1 for the as-synthesized BMnN materials. It can be observed that microwave synthesis produced large needle-like ceramics formed by nanostructured particles, as previously reported in a previous paper, for the isostructural Ba(Mg$_{1/3}$Nb$_{2/3}$)O$_3$ material.[9] For the larger needle displayed in Figure 1 (top inset, SEM), the values of width, length, and aspect ratio are ∼3 μm, ∼90 μm, and 30, respectively. For nanosized particles (bottom inset, TEM), similar aspect ratios apply, but the dimensions are 3 orders of magnitude lower. These results show that the microwave-hydrothermal processing introduces a high anisotropy (with large aspect ratio). Also, each large needle has a nearly uniform shape along its entire length, indicating that the growth anisotropy is strictly maintained throughout the process. Figure 1 shows that the materials exhibit well-faceted crystal ends, without any branching. In previous works, the microwave synthesis was successfully applied for the production of highly anisotropic particles of gold,[18] large aluminum phosphate crystals,[19] and hydroxyapatites.[20] However, the results presented here cannot be explained based on such papers, particularly the production of large materials through "linking" of small particles.

A reduction in surface energy is the primary driving force for crystal growth and morphology evolution. In the present work, the experimental observation can not be explained by the most cited Ostwald ripening process, in which crystal growth is described in terms of growth of larger particles at the expense of the smaller ones.[21] Microwaves have the useful property of heating some materials while leaving others cold.[22,23] Essentially a high-frequency electric field, microwaves cause free ions to displace in the direction of the applied field. Under these conditions, the solvents (water in our case) become superheated, and the precipitation (nucleation) occurs rapidly. This fast
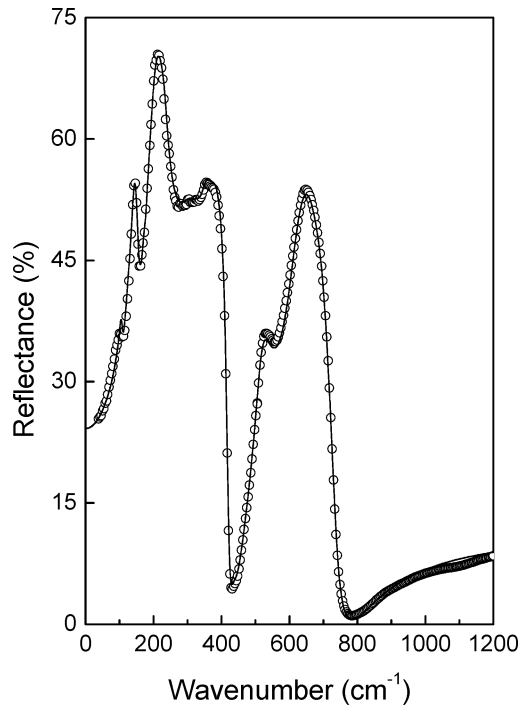
Synthesized Ba(Mn$_{1/3}$Nb$_{2/3}$)O$_3$ Complex Perovskites

J. Phys. Chem. B, Vol. 113, No. 29, 2009 **9751**

Figure 2. Infrared reflectivity spectrum of the Ba(Mn$_{1/3}$Nb$_{2/3}$)O$_3$ ceramic sintered at 1400 °C, for 4 h. Open circles indicate the experimental data, while the solid line represents the calculated reflectivity.

TABLE 1: Dispersion Parameters Calculated from the Fit of the Infrared Reflectance Spectrum of Ba(Mn$_{1/3}$Nb$_{2/3}$)O$_3$[a]

$\Omega_{j,TO}$	$\gamma_{j,TO}$	$\Omega_{j,LO}$	$\gamma_{j,LO}$	$\Delta\varepsilon_j$	$10^8 \tan \delta_j/\omega$
107.8	6.4	108.7	6.9	0.151	968
147.1	13.1	155.0	25.6	0.997	7028
174.9	6.4	175.2	6.3	0.022	53
205.0	23.9	210.0	96.6	0.502	3333
226.7	48.1	236.9	45.6	0.538	5852
306.8	56.6	311.3	53.6	0.304	2129
330.5	55.4	336.0	47.2	0.367	2161
349.1	52.7	367.0	63.8	0.525	2640
383.2	53.4	396.5	55.3	0.190	804
412.6	56.6	419.6	15.5	0.069	265
443.4	19.3	443.5	17.9	0.001	1
451.7	52.9	452.0	41.7	0.004	11
516.6	40.4	517.0	94.1	0.008	14
614.2	78.6	636.5	94.5	0.458	1110
681.7	45.2	683.2	62.9	0.222	2470
684.4	59.9	733.9	44.5	0.161	240
$\varepsilon_\infty = 4.11$		$\varepsilon_r = 8.6$		$\Sigma \tan \delta_j/\omega = 29079 \times 10^{-8}$	

[a] Positions (Ω) and damping constants (γ) are given in cm^{-1}.

nucleation leads to the production of very fine particles, which are now free to move according to the applied electromagnetic fields in the microwave oven. In a second step, the nanostructured particles could undergo a multiplying growth via a "cementing mechanism". Thus, large crystals could be prepared from a direct combination of small crystals, which is also called "oriented attachment".[24–26] Under a microwave-hydrothermal condition, the side crystal planes are able to glue altogether to form larger crystals. This mechanism involves crystal growth by precise, crystallographically controlled addition of primary individual particles.[27] For the samples studied in the present work, the presence of OH$^-$ ions in the strong alkaline aqueous solutions could help oriented attachment under microwaves, allowing an intimate contact between the surface planes.

In terms of its structure, BMnN belongs to a group of oxides with the 1:2 ratio of two B-site ions of unlike valence, Mn^{2+} and Nb^{5+}. As in its analogue compounds with tantalum, the charge compensation requires ordering on the B-site ion distribution, which results in a trigonal quasi-layered structure described by the $P\bar{3}m1$ space group. In the ordered form, the Mn and Nb octahedra are located in the cubic (111) perovskite planes in 1:2 stoichiometric proportions, according to the sequence $-Mn-Nb-Nb-Mn-Nb-Nb-$. Assuming this structure with three formulas per unit cell, $D_{3d}^3(P\bar{3}m1)$, there are 15 atoms in the primitive cell and 45 degrees of freedom. BMnN shows the following Wyckoff site distribution: two barium ions occupy 2d sites and one Ba occupies a 1b site; the two niobium ions are on 2d sites; one manganese ion is on a 1a 4 site; six oxygen ions are on 6i sites; and three O ions are on 3f sites. The distribution of the vibrational modes of the BMnN in terms of the irreducible representations of the D_{3d} factor-group at the Γ-point of the first Brillouin zone is: $A_{2u} + E_u$ (acoustic), $A_{2g} + 2A_{2u}$ (silent), $7A_{2u} + 9E_u$ (infrared), and $4A_{1g} + 5E_g$ (Raman).[28] Thus, up to nine Raman-active bands and 16 infrared-active modes are expected for BMnN ceramic. Figure 2 shows the infrared reflectivity spectrum for the sintered BMnN sample

(open circles). The experimental data were fitted by using a nonlinear least-squares program[29] based upon the four-parameter semiquantum model proposed by Gervais and Piriou.[30] According to this model, the contribution of the infrared modes for the dielectric function is given by the following expression

$$\varepsilon(\omega) = \varepsilon_\infty \prod_{j=1}^N \frac{\Omega_{j,LO}^2 - \omega^2 + i\omega\gamma_{j,LO}}{\Omega_{j,TO}^2 - \omega^2 + i\omega\gamma_{j,TO}} \tag{1}$$

where N is the number of polar modes; $\varepsilon(\omega)$ is the frequency-dependent dielectric function; ε_∞ is the high frequency dielectric constant due to the electronic polarization contribution; $\Omega_{j,LO}(\Omega_{j,TO})$ and $\gamma_{j,LO}(\gamma_{j,TO})$ are the longitudinal (transverse) optical mode frequency and damping constants of the jth mode, respectively. The measured reflectivity spectrum is related to the dielectric function in a quasi-normal incident angle by

$$R = \left| \frac{\sqrt{\varepsilon(\omega)} - 1}{\sqrt{\varepsilon(\omega)} + 1} \right|^2 \tag{2}$$

By using eqs 1 and 2, the measured infrared reflectivity spectrum can be fitted giving up to N pairs of TO–LO modes. The fitting reflectivity spectrum is presented in Figure 2 (solid red line) together with the experimental data, showing a relatively good agreement. The parameters of the 16 optical polar modes obtained from this fit are given in Table 1 in perfect agreement with the group theoretical predictions (16 infrared-active bands). For BMnN, there are three distinct groups of bands:[11] three low-wavenumber bands in the frequency region 100–180 cm^{-1}, which can be attributed to the A–BO$_3$ external mode, nine midwavenumber bands between 180 and 450 cm^{-1} (O–B–O bending modes), and four high-wavenumber bands above 450 cm^{-1}, linked to the oxygen octahedra-elongation modes, that is, BO$_6$ stretching modes. These results expand the only existing infrared data for BMnN,[14] where only five bands were identified.

To determine the contribution of the optical polar phonon modes to the microwave properties of the BMN, we calculate ε_r, $\tan \delta$, and Q in the microwave-frequency range. In these frequencies, $\Omega_{j,TO} \gg \omega$ and the dielectric losses are given by[17]

$$\tan\delta_j = \omega\frac{\Delta\varepsilon_j\gamma_{j,\mathrm{TO}}/\Omega_{j,\mathrm{TO}}^2}{\varepsilon_\infty + \sum\limits_j \Delta\varepsilon_j} \tag{3}$$

where $\Delta\varepsilon_j$ is the oscillator strength of the jth mode and gives the contribution of each oscillation (or polar mode) for the reflectance spectra. This parameter can be described in terms of the optical parameters described above as[17]

$$\Delta\varepsilon_j = \frac{\varepsilon_\infty}{\Omega_{j,\mathrm{TO}}^2} \times \frac{\prod\limits_k (\Omega_{k,\mathrm{LO}}^2 - \Omega_{j,\mathrm{TO}}^2)}{\prod\limits_{k\neq j} (\Omega_{k,\mathrm{TO}}^2 - \Omega_{j,\mathrm{TO}}^2)} \tag{4}$$

The respective values calculated for $\Delta\varepsilon_j$ and $\tan\delta_j$ are given, together with the optical dispersion parameters, in Table 1. The dielectric losses at microwave region can be determined from infrared spectroscopy by $\tan\delta = \sum_j \tan\delta_j$ and coincide with the actual dielectric loss at the microwave frequency if the measurement error is negligible. In the present case, we estimate a Q of the order of

$$Q = \frac{1}{\tan\delta} = 10.4 \times 10^3 \tag{5}$$

at 10 GHz ($\omega = 0.333\ \mathrm{cm^{-1}}$) for our BMnN ceramic. This result confirms BMnN as an adequate-Q microwave material. The real part of the dielectric permittivity ε_r in the microwave-frequency range can be considered as frequency independent and is given by $\varepsilon_r = \varepsilon_\infty + \sum_j \Delta\varepsilon_j$, once $\Omega_{j,\mathrm{TO}} \gg \omega$. For the BMnN ceramics, $\varepsilon_r = 8.6$, which is relatively lower than the minimum value usually required for passive devices employed in electronic microwave circuits (typically $\varepsilon_r > 10$).

Room-temperature Raman analysis was carried out in sintered BMnN ceramics, and the results are displayed in Figure 3 for the 532 nm laser line and 10 mW effective power. As it can be seen, an unexpected low intensity, very noisy spectrum was obtained if compared with those previously observed in similar 1:2 and even 1:1 complex perovskites with Ba ions in the A-site.[8–10,31] In general, the bands are less intense and broader than those commonly observed for materials with similar compositions. Also, extra bands are seen, which could indicate structural disorder. However, the chemical similarity between BMnN and other materials previously studied[8–10] helps us to understand and assign the Raman-active modes. Figure 3 shows nine bands identified after fitting with a sum of Lorentzian lines and assigned according to previous works to vibrational first-order Raman modes (see Table 2).[8–10] Two overlapping bands at 77 and 101 $\mathrm{cm^{-1}}$ are due to A_{1g} (Ba) and E_g (Ba) symmetry modes, while modes associated to oxygen ions occur at 356 and 771 $\mathrm{cm^{-1}}$ (A_{1g}) and 146, 329, and 484 $\mathrm{cm^{-1}}$ (E_g). Bands due to niobium ions occur at 205 $\mathrm{cm^{-1}}$ (E_g) and 292 $\mathrm{cm^{-1}}$ (A_{1g}). The extra bands identified at 415, 533, and 654 $\mathrm{cm^{-1}}$ could be due to disorder or defects, but XRD and infrared results (Figures 1 and 2) indicate fully ordered, single-phase samples. Also, the perfect agreement between group theory approaches and experimental data for both infrared and Raman spectroscopies lead us to conclude that disorder was not responsible for the observed extra Raman bands. Then, we have looked for another physical origin for these modes.

Recently, Fujioka et al.[15,16,32] studied Ba_2MnWO_6 and Sr_2MnWO_6 ceramics and found two different series of resonance-
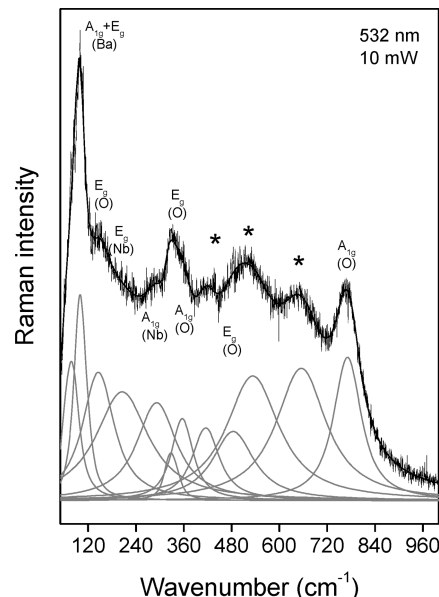
Figure 3. Room-temperature Raman spectrum for the $Ba(Mn_{1/3}Nb_{2/3})O_3$ complex perovskite, obtained with the 532 nm line and 10 mW of effective laser power (power density $8 \times 10^6\ \mathrm{W/cm^2}$). The experimental data were fitted (solid black line) with a sum of Lorentzian curves (gray lines). The assignment of the lattice modes is presented beside three extra modes marked by asterisks.

TABLE 2: Observed Raman Modes for the $Ba(Mn_{1/3}Nb_{2/3})O_3$ Ceramics[a]

band	Ω	γ	assignment
1	76.9	35	A_{1g} (Ba)
2	100.9	27	E_g (Ba)
3	145.6	90	E_g (O)
4	205.3	156	E_g (Nb)
5	291.9	116	A_{1g} (Nb)
6	329.3	26	E_g (O)
7	356.2	57	A_{1g} (O)
8	414.9	76	extra (FC)
9	484.0	121	E_g (O)
10	533.1	157	extra (FC)
11	654.8	149	extra (FC)
12	770.9	78	A_{1g} (O)

[a] Positions (Ω, $\mathrm{cm^{-1}}$) and full width at half-maxima (γ, $\mathrm{cm^{-1}}$) were obtained from the adjustment of the experimental data by Lorentzian lines.

Raman scattering modes as a function of exciting laser. The authors attributed their observations to electron–phonon interactions of Franck–Condon (FC) type. When this mechanism holds, light excites an electron from its ground state to a higher energy state with sufficiently long lifetime for a lattice relaxation. In other words, the FC mechanism activates multiphonon Raman scattering, and electron–phonon interactions appear as a result of comparable lifetimes between excited electrons and moving nuclei during atomic vibrations.[15,32,33] For the double perovskites studied by Fujioka et al., electronic band structure calculations revealed that the valence bands are mainly formed from Mn 3d and O 2p states, while the conduction bands are derived from W 5d and O 2p states.[32] These authors have predicted the formation of localized bands between the valence and the conduction bands edges. Particularly, they showed that two different sets of resonant modes were excited by tuning the laser wavelength: red lines result in resonance modes between 500 and 700 $\mathrm{cm^{-1}}$, while green and blue lines generate bands between 1400 and 1650 $\mathrm{cm^{-1}}$. Also, the FC effect is

Synthesized Ba(Mn$_{1/3}$Nb$_{2/3}$)O$_3$ Complex Perovskites

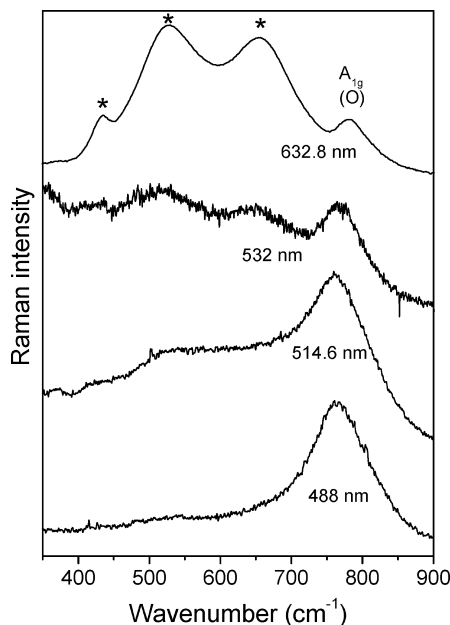*J. Phys. Chem. B, Vol. 113, No. 29, 2009* **9753**

Figure 4. Raman spectra for the BMnN ceramics under different laser excitations: 632.8 nm (6 mW, 8 × 10^6 W/cm^2); 532 nm (10 mW, 8 × 10^6 W/cm^2); 514.5 nm (40 mW, 2.5 × 10^7 W/cm^2); and 488 nm (30 mW, 2.1 × 10^7 W/cm^2). FC modes are marked with asterisks, besides the A_{1g} band at 771 cm^{-1}.

highly enhanced at lower temperatures, once thermal vibrations are detrimental for the effect.

Figure 4 shows the dependence of the room-temperature Raman spectra of BMnN ceramics on the laser wavelength in the range 350−900 cm^{-1}, the region where extra bands identified in Figure 3 appeared (marked by asterisks). As can be seen, the spectra are quite different with huge variation in the intensity of the extra bands. Excitation with the red line (632.8 nm) has produced the stronger FC bands, while higher excitation energies (488 > 514.5 > 532 nm) weaken the electron−phonon interactions. According to electronic band calculations, lower energy excitations (red light) could correspond to electron transfer from the localized Mn 3d band to the conduction band.[32] Practically no extra modes can be identified for the blue line (488 nm). The totally symmetric oxygen breathing mode (A_{1g} at 771 cm^{-1}) increases its relative intensity, as expected for decreasing electron−phonon interactions. Due to e_g−e_g electronic transition of the Mn ions, small displacements of these ions occur, distorting the oxygen octahedra. Thus, the related vibration is no longer totally symmetric, which affects the intensity of the A_{1g} mode at 771 cm^{-1}. The extra modes located at 414, 533, and 654 cm^{-1} appeared equidistantly (approximately 120 cm^{-1}), which corroborates the assumption of electronic transitions in BMnN ceramics. According to Fujioka et al.,[32] the extra mode energies being integer multiples of a fundamental frequency could be related to the formation of a polaron, i.e., a lattice distortion accompanied by a low mobility electron.

Figure 5 shows for the two highest-energy excitation lines (514.5 and 488 nm) the influence of the laser power in the Raman spectra of BMnN samples, maintaining other experimental conditions (room temperature, 80× objective). For both green (514.5 nm) and blue (488 nm) lines, a weakening of the electron−phonon interactions for increasing laser powers was observed. FC modes are still present under green line excitation at 40 mW, disappearing when the power level was increased to 50 mW. For the blue line (488 nm), multiphonon Raman scattering is absent when the laser power is higher than 30 mW. These results could be interpreted as derived from heating of
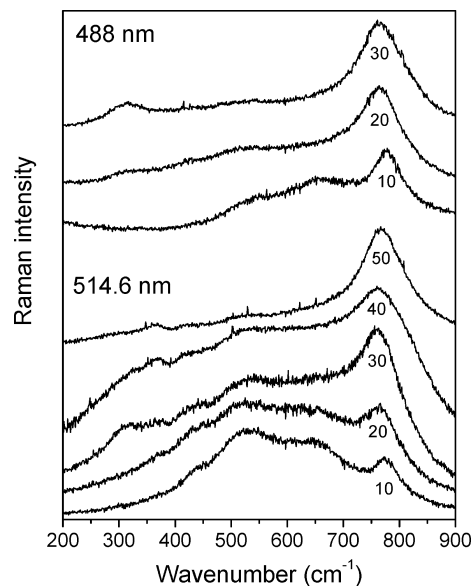

Figure 5. Raman spectra for the BMnN ceramics under green (514.5 nm) and blue (488 nm) excitation lines for different laser powers (in mW). The power densities for 10 mW power were 6.2 × 10^6 W/cm^2 and 6.9 × 10^6 W/cm^2 for green and blue lines, respectively.
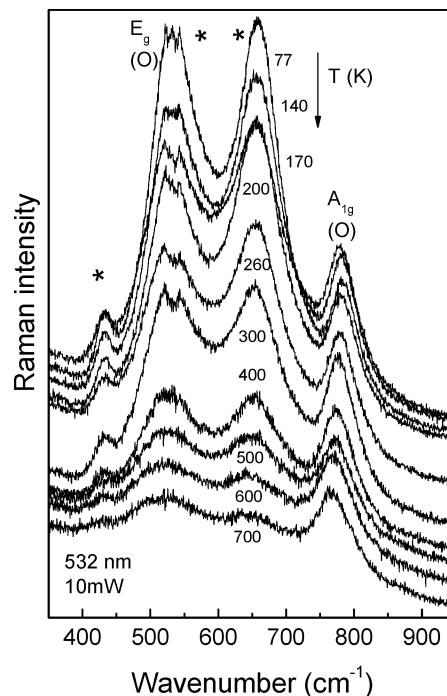

Figure 6. Temperature dependence of the FC modes for the BMnN ceramics. The Raman scattering was conducted under a green excitation line (532 nm) and 10 mW laser power (8.6 × 10^5 W/cm^2). Temperatures are indicated in K.

the sample for increasing laser powers. In this respect, Figure 6 shows the dependence of the heating temperature on the FC modes for Raman scattering experiments carried out with a 532 nm excitation line and 10 mW of laser power (20× objective). As can be seen, the electron−phonon interactions are stronger and stronger for decreasing temperatures, as expected. This phenomenon is due to decreasing influence of anharmonicity and thermal vibrations, which also lead to narrowing of the bands.[16] Figure 7 shows the intensity ratio between the extra FC band at 654 cm^{-1} and the totally symmetric A_{1g} mode at
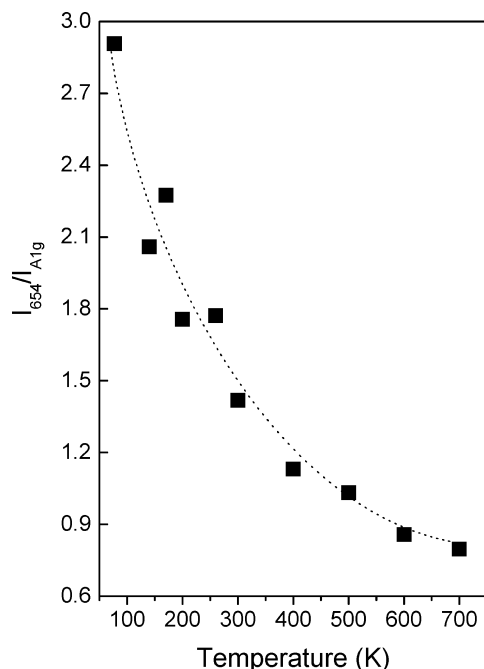
Figure 7. Intensity ratio between the extra FC band at 654 cm^{-1} and the totally symmetric A_{1g} stretching mode (771 cm^{-1}) extracted from data of the preceding figure. The dotted line is a guide for the eyes.
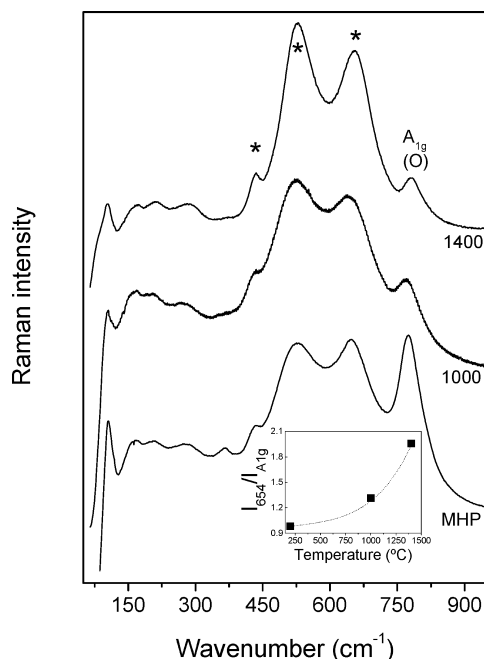

Figure 8. Room-temperature Raman spectra for the BMnN samples as a function of processing temperature: as-synthesized MHP, calcined powders at 1000 °C, and sintered ceramics at 1400 °C. The spectra were obtained with the 632.8 nm laser line (6 mW, 8 × 10^6 W/cm^2). Inset: intensity ratio between the FC band at 654 cm^{-1} and the A_{1g} mode (771 cm^{-1}). The dotted line is a guide for the eyes.

771 cm^{-1}, as a function of heating temperature. The enhancement of the electron−phonon interactions of FC origin becomes clear.

Finally, Figure 8 shows the Raman spectra of BMnN samples under a red excitation line (632.8 nm) as a function of processing conditions: as-synthesized microwave-hydrothermal powders (MHP), calcined powders at 1000 °C, and sintered ceramics at 1400 °C. The intensity ratio between the FC mode at 654 cm^{-1} and the A_{1g} (O) band around 771 cm^{-1} was plotted as a function

of processing temperature (Figure 8, inset), where the increase in the electron−phonon interactions for increasing processing temperature can be observed. As recently observed in similar microwave-hydrothermal ceramics,[8] there is a notable influence of the heating temperature on the degree of ordering in complex perovskites, with resulting changes in the behavior of vibrational modes. It is believed that our samples present the same features, which could lead to a different multiphonon response. MHPs are likely more disordered than the sintered ceramic, with B-site ions in relative disagreement with the ideal proportion 1:2. Thus, the FC mechanism could not activate the multiphonon Raman scattering as efficiently as in sintered, fully ordered structures.

4. Conclusions

Microwave-hydrothermal synthesis was employed to produce crystalline, single-phase Ba(Mn$_{1/3}$Nb$_{2/3}$)O$_3$ materials for the first time. Large needle-like ceramics with high anisotropy and aspect ratio were obtained. The use of microwaves leads to fast nucleation and production of nanosized particles, which could undergo a multiplying growth via a "cementing mechanism". Hence, large crystals could be prepared from a direct combination of small crystals (oriented attachment). Infrared and Raman spectroscopies showed perfect agreement with group-theoretical predictions for a trigonal, $P\bar{3}m1$ structure where, respectively, 16 and 9 bands were predicted and observed experimentally. Extra modes were identified in Raman scattering experiments conducted in different wavelengths, laser powers, and temperatures. The results showed that multiphonon Raman features due to the Franck−Condon mechanism can be activated and controlled in the Raman spectra. It can be concluded that Mn ions play a peculiar role in the lattice dynamics of the BMnN ceramic system by presenting electronic excitations that can distort the crystal lattice, as also observed in double complex perovskites.

References and Notes

(1) Mitchell, R. H. *Perovskites modern and ancient*; Almaz Press: Ontario, 2002; *Properties and applications of perovskite type oxides*; Marcel Decker: New York, 1993.
(2) Samara, G. A. *J. Phys.: Condens. Matter* **2003**, *15*, R367.
(3) Blackstead, H. A.; Dow, J. D.; Harshman, D. R.; Yelon, W. B.; Chen, M. X.; Wu, M. K.; Chen, D. Y.; Chien, F. Z.; Pulling, D. B. *Phys. Rev. B* **2001**, *61*, 214412.
(4) Bokov, A. A.; Ye, Z. G. *J. Mater. Sci.* **2006**, *41*, 31.
(5) Wojtowicz, A. J.; Drozdowski, W.; Wisniewski, D.; Lefaucheur, J. L.; Galazka, Z.; Gou, Z. H.; Lukasiewicz, T.; Kisielewski, J. *Opt. Mater.* **2006**, *28*, 85.
(6) Osterloh, F. E. *Chem. Mater.* **2008**, *20*, 35.
(7) Reaney, I. M.; Iddles, D. *J. Am. Ceram. Soc.* **2006**, *89*, 2063.
(8) Dias, A.; Sá, R. G.; Moreira, R. L. *J. Raman Spectrosc.* **2008**, *39*, 1805.
(9) Dias, A.; Matinaga, F. M.; Moreira, R. L. *Chem. Mater.* **2007**, *19*, 2335.
(10) Moreira, R. L.; Dias, A. *J. Eur. Ceram. Soc.* **2005**, *25*, 2843.
(11) Dias, A.; Moreira, R. L. *J. Appl. Phys.* **2003**, *94*, 3414.
(12) Dias, A.; Ciminelli, V. S. T. *Chem. Mater.* **2003**, *15*, 1344.
(13) Liu, Y.; Withers, R. L.; Whichello, A. P.; Norén, L.; Ting, V.; Brink, F.; FitzGerald, J. D. *J. Solid State Chem.* **2005**, *178*, 3389.
(14) Tochi, K.; Ohgaku, T.; Takeuchi, N.; Emura, S. *J. Ceram. Soc. Jpn.* **1989**, *97*, 875.
(15) Fujioka, Y.; Frantti, J.; Kakihana, M. *J. Phys. Chem. B* **2004**, *108*, 17012.
(16) Fujioka, Y.; Frantti, J.; Kakihana, M. *J. Phys. Chem. B* **2006**, *110*, 777.

(17) Hayes W.; Loudon, R. *Scattering of light by crystals*; Wiley: New York, 1978.

(18) Liu, F. K.; Chang, Y. C.; Ko, F. H.; Chu, T. C. *Mater. Lett.* **2004**, *58*, 373.

(19) Girnus, I.; Jancke, K.; Vetter, R.; Richter-Mendau, J.; Caro, J. *Zeolites* **1995**, *15*, 33.

(20) Siddharthan, A.; Seshadri, S. K.; Sampath Kumar, T. S. *Scripta Mater.* **2006**, *55*, 175.

(21) Baldan, A. *J. Mater. Sci.* **2002**, *37*, 2171.

(22) Adam, D. *Nature* **2003**, *421*, 571.

(23) Bergese, P. *Acta Mater.* **2006**, *54*, 1843.

(24) Zhang, H. Z.; Banfield, J. F. *Chem. Mater.* **2002**, *14*, 4145.

(25) Pacholski, C.; Kornowski, A.; Weller, H. *Angew. Chem., Int. Ed.* **2002**, *41*, 1188.

(26) Sampanthar, J. T.; Zeng, H. C. *J. Am. Chem. Soc.* **2002**, *124*, 6668.

(27) Hu, X. L.; Zhu, Y. J.; Wang, S. W. *Mater. Chem. Phys.* **2004**, *88*, 421.

(28) Rousseau, D. L.; Bauman, R. P.; Porto, S. P. S. *J. Raman Spectrosc.* **1981**, *10*, 253.

(29) Meneses, D. D.; Gruener, G.; Malki, M.; Echegut, P. *J. Non-Cryst. Solids* **2005**, *351*, 124.

(30) Gervais, F.; Piriou, B. *Phys. Rev. B* **1974**, *10*, 1642.

(31) Dias, A.; Khalam, L. A.; Sebastian, M. T.; Paschoal, C. W. A.; Moreira, R. L. *Chem. Mater.* **2006**, *18*, 214.

(32) Fujioka, Y.; Frantti, J.; Nieminen, R. M. *J. Phys. Chem. B* **2008**, *112*, 6742.

(33) Perebeinos, V.; Allen, P. B. *Phys. Rev. B* **2001**, *64*, 085118.

JP902616A